For submission to Water, Air, & Soil Pollution

The kinetics of aqueous mercury(II) reduction by sulfite over an array of environmental conditions

Aryeh I. Feinberg, Uday Kurien and Parisa A. Ariya*

Department of Chemistry and Department of Atmospheric and Oceanic Sciences, McGill University

801 Sherbrooke St. W., Montreal, QC, CANADA, H3A 2K6

Tel: (514) 398-6931 Fax: (514) 398-3797

Emails: aryeh.feinberg@mail.mcgill.ca;uday.kurien@mail.mcgill.ca; parisa.ariya@mcgill.ca

** Corresponding author*

Abstract

The reaction of Hg^{2+} with sulfite is a major identified reduction pathway in the atmosphere. UV absorption spectroscopy was used to study the kinetics of Hg^{2+} reduction by sulfite (Na_2SO_3) in the presence of fly ash. Upon the addition of Cumberland and Shawnee fly ash samples, the reduction rates were 0.0071 ± 0.0008 s^{-1} and 0.0009 ± 0.0006 s^{-1}, respectively. This represents *c.a.* 40% and 90% decreases in the homogeneous rate, 0.013 ± 0.007 s^{-1}. The reduction reaction was also observed when Cumberland was added without Na_2SO_3. Sulfur elemental analyzer and high-resolution field emission scanning microscopy with energy dispersive X-ray spectroscopy (HR-FE-SEM-EDS) characterization confirmed that Cumberland fly ash particles were rich in sulfur. Nanoparticle Tracking Analysis (NTA) determined the mean particle size in solution to be 246 ± 25 nm for Cumberland fly ash and 198 ± 14 nm for Shawnee. To obtain further insight on observed Hg^{2+} homogeneous reduction rates by sulfite, the effects of several environmental variables were investigated. $Hg(NO_3)_2$ and HgO were used as the sources of Hg^{2+}. Extended pH (1 – 7) and temperature (1.0 – 45.0 °C) ranges were studied for the first time. The enthalpies of activation for the HgO reduction were 94 ± 3 kJ mol^{-1} at pH 1 and 92 ± 4 kJ mol^{-1} at pH 3, while the entropies were 33 ± 9 J mol^{-1} K^{-1} at pH 1 and 30 ± 10 J mol^{-1} K^{-1} at pH 3. It was determined that increasing ionic strength, especially with nitrate species, slows down the reaction at pH = 7. Significance of the results on the variability of mercury reduction by sulfite at various environmental conditions, and its implication in modelling are discussed.

1. Introduction

Mercury is a toxic trace metal whose major anthropogenic source is coal combustion. Because the dependence on coal globally as a source of energy is increasing, the issue of mercury emissions is pressing. In its oxidized form mercury can dissolve in water and be transformed by bacteria into methyl mercury (Morel *et al.*, 1998). This methylated form of mercury is propagated through the aquatic food chain, leading to toxic levels of mercury in fish. Fish consumption has caused massive outbreaks of neurological diseases in the past (Davidson *et al.*, 2004; Engler, 1985). The 2013 Minamata Convention, which until now has been signed by 120 countries, established a global commitment to decrease mercury emissions (Selin, 2014).

Mercury is operationally defined to have three major forms: elemental mercury (Hg^0), oxidized mercury (Hg^{2+}) and particulate-bound mercury (Hg_p) (Wilcox *et al.*, 2012). Understanding the speciation of mercury is crucial, as each form behaves differently in the environment. Hg^{2+} is methylated by bacteria, meaning its concentration will determine the amount of bioavailable mercury (Fitzgerald *et al.*, 2007). Hg^0 has been assumed to have a long atmospheric lifetime (0.5-2 years) and can be transported for long distances, creating a global-scale issue (Lamborg *et al.*, 2002). However, in the polar regions and over salt lakes such as the Dead Sea, a much shorter lifetime has been observed (Ariya *et al.*, 2004; Ebinghaus *et al.*, 2002).

Much research has gone into the oxidation reactions of mercury (Senior *et al.*, 2000; Wilcox *et al.*, 2012), however environmental reduction pathways have been less investigated (Ariya *et al.*, 2009). Van Loon *et al.* (2000) found that aqueous sulfite reduces HgO to Hg^0 via formation of the $HgSO_3$ complex. When Hg^{2+} and Hg^0 are combined in solution, they react in a comproportionation reaction:

$$Hg^{2+}_{(aq)} + Hg^0_{(aq)} \rightleftharpoons Hg_2^{2+}_{(aq)} \quad (1)$$

This reaction is rapid, with a bimolecular rate constant of 5.9×10^8 M^{-1} s^{-1} and an equilibrium constant 1.8×10^8 M^{-1} (Clever *et al.*, 1985). Therefore, the Hg^0 that is formed in the reduction can be trapped by excess Hg^{2+} to produce Hg_2^{2+}, which absorbs UV radiation (Van Loon *et al.*, 2000). The kinetics of this reaction can be monitored using UV spectroscopy.

Several environmental factors affecting the reaction, such as using different Hg^{2+} complexes, varying ions to test ionic strength, and an increased pH range, have not been studied. Furthermore, the understanding of mercury reactions at surfaces is scarce (Ariya *et al.*, 2009).

The possibility of the aqueous sulfite reduction pathway occurring in the liquid layers of aerosols or cloud surfaces has been acknowledged (Deeds *et al.*, 2013). The presence of environmental surfaces can drastically change the rate of homogeneous reactions (Amirbahman *et al.*, 2013).

More than 420 million tons of fly ash are produced globally per year in the coal combustion process (Wilcox *et al.*, 2012). Fly ash could be an important surface for mercury reactions in industrial stacks and contaminated aquatic systems. Some of the components of fly ash have been associated with reduction of Hg^{2+} in aqueous systems. Hematite (Fe_2O_3) and magnetite (Fe_3O_4) accelerated Hg^{2+} reduction by Fe^{2+} compared to the homogeneous rate, whereas γ-alumina (Al_2O_3) decreased the reduction rate (Amirbahman et al., 2013; Wiatrowski et al., 2009). Loss of Hg^{2+} by reduction and adsorption has also been observed in aqueous solutions containing activated carbon (Huang and Blankenship, 1984; Sen and De, 1987). Therefore, iron oxides, γ-alumina, and carbon contents could all be important parameters in determining the reduction capabilities of fly ash.

The present work aims to address two objectives. Firstly, we explored the effect of heterogeneity on kinetic reduction rates by using two different batches of fly ash added to the Hg^{2+} solution. To interpret the results of this experiment, we expanded the current understanding of the mercury reduction by sulfite. $Hg(NO_3)_2$ along with HgO were used as the sources of Hg^{2+}. The reaction kinetics was investigated under a relatively broad range of temperature and pH. The effect of using different species in testing the ionic strength effect was evaluated. The results of these novel experiments will establish new limitations and possibilities for the extent of Hg^{2+} reduction by sulfite in aqueous systems.

2. Experimental Section

2.1. Chemicals

All solutions were prepared using Milli-Q water (18.2 MΩ cm at 25 °C). The 0.1 M HgO stock solution was made by dissolving red HgO (Sigma-Aldrich, >99%) in 0.059 M $HClO_4$ (Fisher, 60%). A neutral 0.1 M $Hg(NO_3)_2$ solution was prepared by dissolving $Hg(NO_3)_2$ (Fisher, >98%) in water. The exact concentrations of the mercuric ion solutions were determined by titration with standard 0.005 M KSCN (EMD BioSciences Inc, >99%) solution. 0.07 M ferric alum ($NH_4Fe(SO_4)_2 \bullet 12\ H_2O$) in 1.94 M HNO_3 (Sigma-Aldrich, 70%) was used to determine the

endpoint (Malisoff and Anding Jr, 1935; Van Loon *et al.*, 2000). Na_2SO_3 (Fisher, >98%, anhydrous) solutions were prepared fresh before use to avoid trace-metal catalyzed autoxidation (Hayon *et al.*, 1972; Van Loon *et al.*, 2000). Solutions were stored in airtight sample vials.

Two different fly ash samples were obtained for heterogeneous sulfite reduction. The Cumberland Power Plant (Tennessee) sample was produced in Cumberland Units 1 & 2, which are 1250 MW units. The fuel blend is 70% Illinois Basin (bituminous) and 30% Uinta Basin (subbituminous). The other sample comes from the Shawnee Fossil Plant (Kentucky), which burns a coal blend of 65% Powder River Basin subbituminous coal and 35% Uinta Basin.

2.2. Homogeneous experiments

To characterize the product of the reduction reaction, Hg_2^{2+}, the HgO stock solution was mixed with liquid Hg^0 (Sigma-Aldrich, 99.9995%) overnight. The aqueous phase, composed of Hg_2^{2+}, was separated and its UV spectrum was recorded (Fujita *et al.*, 1973; Higginson, 1951; Van Loon *et al.*, 2000).

The kinetics experiments were conducted using a temperature-controlled Cary 100 spectrophotometer. The scan speed was set to 300 nm/min, with a 0.5 nm resolution. The basic procedure involved filling a square quartz cuvette with diluted (350 μM) HgO or $Hg(NO_3)_2$ solution. The filled cuvette was equilibrated to the desired temperature for 10 minutes. The Na_2SO_3 solution (10 – 60 μM) was added directly before the kinetics scan was initiated on the program. The absorbance data at 236 nm was fit to the first-order integrated rate equation to obtain the rate constant, k (Houston, 2001):

$$A_t = A_0 + (A_\infty - A_0)\,(1 - e^{-kt}) \qquad (2)$$

The reactions were performed at pH 1 and 3 for HgO and pH 1, 3, 5, and 7 for $Hg(NO_3)_2$, using $HClO_4$ to adjust the solution acidity. The temperature in the cuvette cell was varied from 1.0 °C to 45.0 °C. At temperatures higher than 35 °C only the absorbance at 236 nm was monitored, as the reaction rate was too fast to scan multiple wavelengths. The effect of ionic strength on the reaction was tested by addition of $NaClO_4$ (Sigma-Aldrich, >98%), $NaNO_3$ (Anachemia, >99%), and KNO_3 (Fisher, >99%). Due to spectral interferences at 236 nm from nitrate ions, the rate constants in solutions with raised ionic strength were determined from absorbance data at 258 nm. Argon-saturated solutions were prepared by bubbling Ar through Milli-Q water for 30 min.

2.3. Heterogeneous experiments

Before use, fly ash samples were heated at 100 °C for more than 2 h to remove moisture. For more controlled experimental conditions, we homogenized the fly ash samples by grinding them using a mortar and pestle. The two fly ash samples were characterized using the high-resolution Inspect F-50 Field Emission Scanning Electron Microscope (FE-SEM) coupled with energy-dispersive X-ray spectroscopy (EDS). Several fields of view were selected for each sample. The Sulfur content of 5 different samples of each type of fly ash, pre and post heating, was analyzed using a Carbon-Sulfur analyzer (ELTRA CS-800). Briefly, the powder samples (150 mg) were heated with an accelerator (1 g each of Iron and Tungsten) in an inductive furnace maintained under a pure oxygen environment and the oxidized sulfur (SO_2) was measured in an infrared cell. The detection limit of the ELTRA CS-800 for sulfur is ± 0.06%. Nanoparticle Tracking Analysis (NTA) was performed with aqueous suspensions of the fly ash using the NS300 (NanoSight). Ten minute-long videos were recorded for each batch, which were analyzed statistically by the NanoSight software version 2.3 (Gallego-Urrea *et al.*, 2010).

In order to determine the effect of the two fly ash samples on aqueous Hg^{2+} reduction, aqueous suspensions of 0.55 g L^{-1} fly ash were prepared. The stock solution of $Hg(NO_3)_2$ was diluted in the suspension to yield an $Hg(NO_3)_2$ concentration of 350 μM. For some of the experiments 15 μM Na_2SO_3 were also added to the cuvette. The absorbance of the solution was recorded over time in a Cary 50 spectrophotometer at ambient room temperature (28 ± 2 °C). Due to settling of the fly ash particles, the baseline of the absorbance spectrum decreased over the course of the experiment. A corrected absorbance value (A^*) at 236 nm is therefore used:

$$A^* = A_{236nm} - A_{300nm} \quad (3)$$

A^* is substituted in Equation 2 to yield the rate constant in the presence of fly ash. Four replicate trials were conducted for each type of heterogeneous experiment.

3. Results and Discussion

3.1. Reduction of Hg(II) in the Presence of Fly Ash

3.1.1. Size Distribution of Fly Ash

The size of nanoparticles is a crucial factor in determining their reactivity (Burda *et al.*, 2005). By drying and grinding the fly ash samples before use in experiments, we attempted to ensure that the particles were of more similar sizes and shapes. The NTA and FE-SEM characterization that were performed reveal the level of heterogeneity in the sample.

NTA is a technique that can quantify particles in the 10 nm to 2000 nm size range. The size distributions of the Shawnee and Cumberland fly ash samples are displayed in Figure 1. The concentrations of Cumberland and Shawnee particles were $(8.2 \pm 0.5) \times 10^7$ particles mL^{-1} and $(1.12 \pm 0.15) \times 10^8$ particles mL^{-1}, respectively. The mean particle size for the Cumberland batch was 246 ± 25 nm, whereas the mean particle size for Shawnee was 198 ± 14 nm. Hence, the Shawnee particles were on average smaller and have a narrower size distribution. From both distributions it appears that most of the particles are concentrated in the < 400 nm size range. One would expect to see larger particles (> 1 μm) in the size distribution from the FE-SEM images, which showed particles up to 10 μm in diameter. However, it is plausible that larger particles fragmented through agitation of the aqueous solution. The confirmed presence of nanoparticles in the reaction mixtures indicates that heterogeneous interactions are likely.

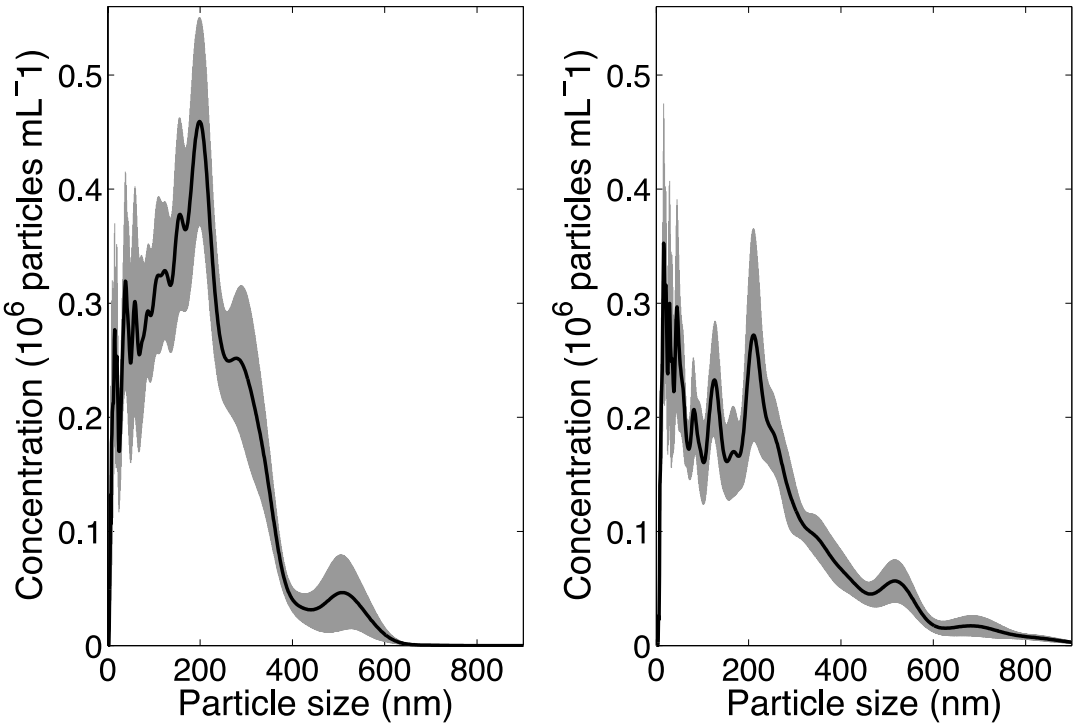

Fig. 1 Particle size distribution for 0.55 g L^{-1} suspensions of A) Shawnee and B) Cumberland fly ash

3.1.2. Physical/Chemical Characterization of Fly Ash

Chemical and physical characterization of the fly ash was performed using FE-SEM/EDS. As extensive FE-SEM/EDS studies have previously been conducted (Kutchko and Kim, 2006), these experiments were only meant to be a cursory examination of the possible chemical differences between the two fly ash batches. Particles were observed from 200 nm to 20 μm in diameter. The major elemental constituents (by weight %) of the fly ash were O, Al, Ca, and Si. Some of the particles (Figure S5) in both batches had high relative concentrations of Fe (up to 8%). These major elements usually comprise minerals such as SiO_2, Al_2O_3, $Al_6Si_2O_{13}$, Fe_2O_3, Fe_3O_4, and CaO (Kutchko and Kim, 2006; Vassilev and Vassileva, 2007).

Several significant chemical differences were found between the Cumberland and Shawnee fly ash particles. Sulfur-rich particles (up to 20%) were detected in the Cumberland batch, as shown in Figure 2. However, none of the recorded Shawnee particles had significant concentrations of sulfur. Increased sulfur concentrations were associated with increased calcium concentrations, in agreement with previous observations by Kutchko and Kim (2006). One particle of fly ash can contain regions with very different compositions and morphologies. Figure 3 displays a Shawnee fly ash particle with a carbon-rich area at the top of the particle (Spectrum 1) and a more common Al/Si/Ca area at the equator of the particle (Spectrum 2). An obvious challenge to characterizing fly ash through FE-SEM/EDS is the degree of heterogeneity that exists between particles in the same sample and in the particle itself. It is also unknown how the morphologies and sizes of these particles would change once they are suspended in the aqueous phase, due to possible agglomeration or splitting of particles.

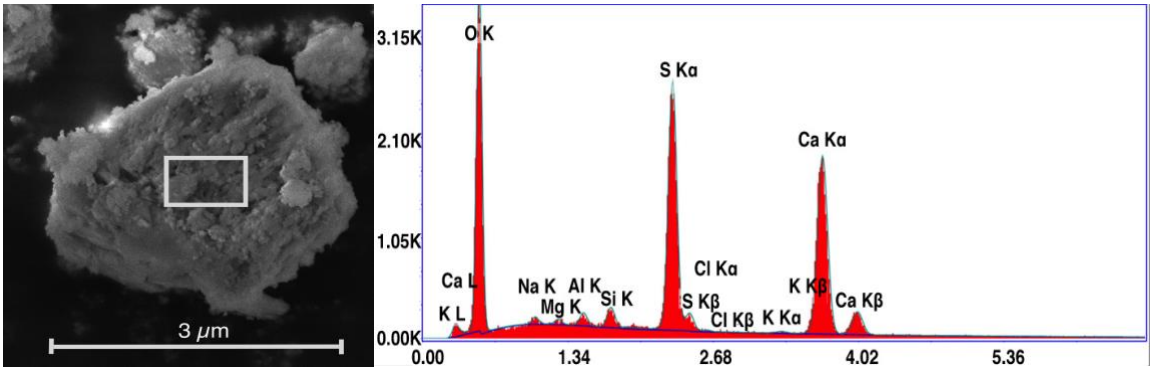

Fig. 2 FE-SEM image/EDS spectrum of Cumberland fly ash particle that is relatively rich in S and Ca

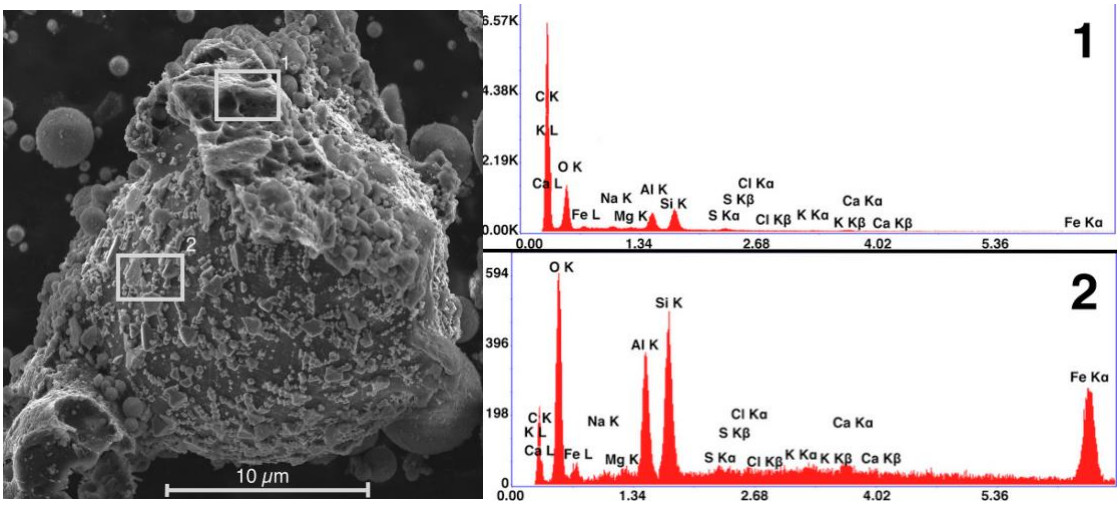

Fig. 3 FE-SEM image/EDS spectrum of Shawnee fly ash particle that has carbon-rich areas on the surface (Spectrum 1) and some regions where Al, Si, and Ca are abundant (Spectrum 2)

To overcome the challenges posed by the heterogeneous nature of fly ash, and to obtain representative sulfur concentrations for each of the different fly ash samples, selective sulfur analysis was also performed using an ELTRA CS-800. From the analysis (shown in supplemental information), it is evident that Cumberland has greater sulfur content (c.a. 1.0%) than Shawnee (c.a. 0.3%) fly ash. This difference in Sulfur content may be a consequence of the coal blends used, with Cumberland using a higher percentage (c.a. 70%) of bituminous coal in the blend. Note that the sulfur content of the fly ash did not change outside experimental uncertainties (Figure S8), when it was heated to remove moisture prior to conducting heterogeneous experiments.

3.1.3. Kinetics

The UV absorption method for measuring the kinetics of Hg^{2+} reduction has been discussed in detail by Van Loon *et al.* (2000). The Supplementary Information section contains information on the method of measuring the rate of Hg_2^{2+} formation over time.

Due to their ubiquity in atmospheric aerosols and aquatic systems (Eriksen *et al.*, 2013; Pósfai *et al.*, 1999), the effect of fly ash on Hg^{2+} reduction by sulfite would be important under environmental conditions. In the absence of fly ash, the homogeneous reduction of $Hg(NO_3)_2$ by

sulfite at pH 7 had a first order rate constant of 0.013 ± 0.007 s^{-1} (Figure 4). When Cumberland fly ash was added to $Hg(NO_3)_2$, without the addition of Na_2SO_3, reduction to Hg_2^{2+} was observed. The rate of reduction was 0.008 ± 0.002 s^{-1}, similar to the rate when Na_2SO_3 was added, 0.0071 ± 0.0008 s^{-1}. In contrast, Hg^{2+} reduction was not observed when Shawnee fly ash was added to $Hg(NO_3)_2$ in the absence of Na_2SO_3. Upon addition of Na_2SO_3 to the Shawnee suspension, the rate constant was greatly reduced from the homogeneous case, 0.0009 ± 0.0006 s^{-1}.

Iron oxides such as magnetite and hematite, which have been shown to promote reduction of $Hg^{2+}_{(aq)}$ (Amirbahman *et al.*, 2013; Wiatrowski *et al.*, 2009), are not expected to be the reason behind the reduction of $Hg(NO_3)_2$ by Cumberland in the absence of Na_2SO_3. Iron was present in similar concentrations in both Cumberland and Shawnee fly ash particles.

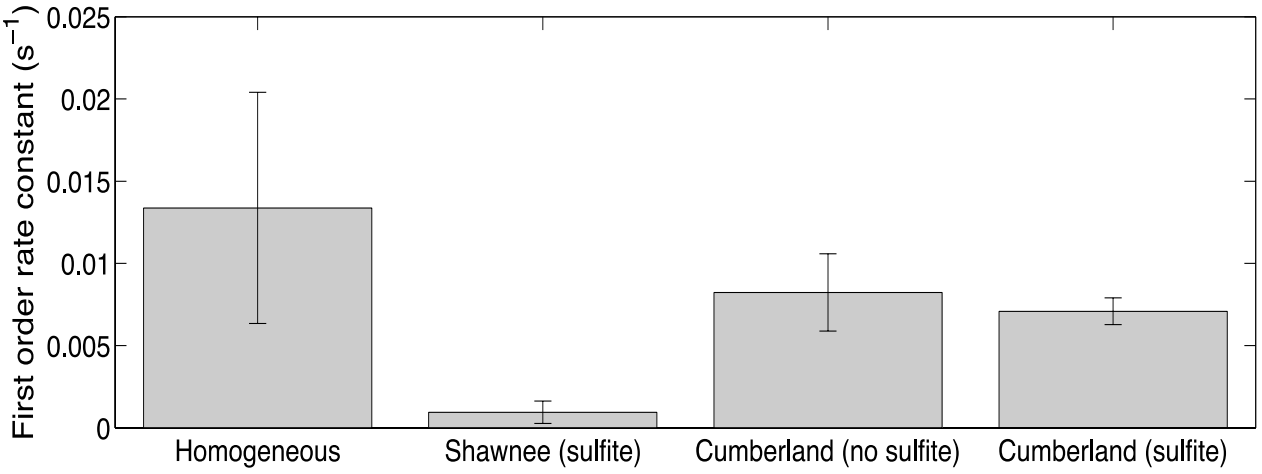

Fig. 4 Effect of the fly ash batches on the rate constant of $Hg(NO_3)_2$ reduction by sulfite at pH 7, T = 301 ± 2 K

The reduction of Hg^{2+} by Cumberland without the addition of sulfite could be explained by sulfite that leaches from the particles into the solution. Sulfur-rich particles were observed in the EDS spectra of the Cumberland batch (Figure 2). Little sulfur was observed in the Shawnee particles, which supports the absence of reduction when only Shawnee fly ash and $Hg(NO_3)_2$ were present in the mixture. The difference in sulfur content of both types of fly ash was further confirmed by sulfur analysis using the ELTRA CS-800 (supplementary data). The Cumberland results demonstrates lends support to the idea that fly ash particles can act as a source of sulfite in aqueous systems, leading to Hg^{2+} reduction. Tong *et al.* (2014) observed that a soluble component of fly ash could be responsible for the reduction of mercury on fly ash surfaces.

More types of fly ash must be tested to determine whether the sulfite leaching is unique to Cumberland fly ash or a more general phenomenon.

In the homogeneous experiments, the reaction rate was found to be independent of sulfite in the concentration range of 10 – 60 μM, with Hg^{2+} being in excess. As seen in Figure 4, the rate of reduction for the Cumberland fly ash mixture was not significantly altered when sulfite was added, suggesting that perhaps the total amount of sulfite lies in this concentration range. Munthe *et al.* (1991) observed different behaviour when sulfite is in excess of Hg^{2+}, with the reduction rate being independent of temperature and dependent on sulfite concentration. Additionally, there are probably several species of sulfur present in the heterogeneous solutions, as some of the known sulfur-compounds in fly ash are sulfates, like $CaSO_4$ (Kutchko and Kim, 2006). Sulfur partitioning reactions could therefore occur once sulfite is added to the fly ash mixture. Further work, particularly on sulfur partitioning is needed to better understand the system, especially more chemical analysis of the soluble components of fly ash.

The 40% and 90% decreases in reaction rate in the presences of Cumberland fly ash and Shawnee fly ash, respectively, could be due to a component of fly ash that absorbs Hg^{2+} (Figure 4). Al_2O_3, a major component of fly ash, may adsorb Hg^{2+}, decreasing the rate of reduction in the aqueous phase (Amirbahman et al., 2013). The unburned carbon in fly ash is also a potential adsorbent of $Hg^{2+}_{(aq)}$. Several studies have found that activated carbon removes a high percentage of $Hg^{2+}_{(aq)}$ at pH 7 (Huang and Blankenship, 1984; Namasivayam and Kadirvelu, 1999; Yardim *et al.*, 2003). More in-depth chemical characterization is required to conclude if Shawnee fly ash contains a higher unburned carbon content than Cumberland, leading to more Hg^{2+} adsorption and slower reduction rates.

Since we hypothesize that leaching of sulfite from Cumberland caused the Hg^{2+} reduction, a further investigation into the homogeneous reduction reaction was warranted. More variables were tested in the homogeneous case to determine possible reasons behind the reduction of the rate constant in the presence of fly ash. Motivated by the results in the heterogeneous case, the dependence of the homogeneous reaction on temperature, pH, and ionic strength studies were extended from the only previous work.

3.2. Homogeneously initiated reduction reaction of Hg(II) by sulfite

3.2.1. pH Dependence

For both HgO and $Hg(NO_3)_2$, the rate was accelerated as the pH was reduced from 3 to 1 (Table 1). The rate of reduction changes linearly with concentration of acid between pH 1 and 3, when ionic strength is kept constant at 1.0 – 1.1 M (Figure S6, Equation S3). The acid-catalyzed path is presumed to involve the protonated intermediate $HgSO_3H^+$ (Van Loon *et al.*, 2000).

Due to its increased solubility, $Hg(NO_3)_2$ is more convenient than HgO for experiments at a wider range of pH values. Although previous work focused solely on the reaction at pH < 3 (Van Loon *et al.*, 2000), this experiment also monitored the reaction at pH 5 and pH 7, in order to provide data for a larger array of environmentally relevant conditions. The rate constant at pH 5 and pH 7 is lower than at pH 3 ($p < 0.002$) at 25 °C (Table 1). This behaviour is not described by the linear relationship in Figure S6, as the acid-catalyzed path was only significant for pH < 2. At the 95% confidence level, one cannot distinguish between the rate constant at pH 5 and pH 7. Previous thermodynamic work has indicated that $Hg(OH)_2$ becomes important as the dominate Hg^{2+} species at these pH levels (Amirbahman *et al.*, 2013). One might expect this to inhibit the formation of Hg_2^{2+} and result in volatilization of gaseous Hg^0 instead. However, the yield of Hg_2^{2+}, as determined by the change of absorbance at 236 nm, was similar between pH 3 and pH 7. Therefore the kinetic analysis is valid for the pH range studied.

By expanding the pH range up to pH 7, these experiments reveal that sulfite reduction of Hg^{2+} is feasible under both acidic and neutral conditions. This covers a wide range of environmental settings, as most of the water in the atmosphere ranges from pH 3 – 5 (Pehkonen and Lin, 1998).

3.2.2. Temperature Dependence

Activation parameters can be extracted from the temperature data using the Eyring-Polanyi equation (Evans and Polanyi, 1935):

$$\ln \frac{k}{T} = - \frac{\Delta H^{\ddagger}}{RT} + \ln \frac{k_B}{h} + \frac{\Delta S^{\ddagger}}{R} \qquad (4)$$

A plot of ln (k/T) versus T^{-1} should be linear with a slope of $-\Delta H^{\ddagger}/R$ and an intercept of $\ln(k_B/h) + \Delta S^{\ddagger}/R$.

The reduction reaction was highly temperature dependent for both HgO and $Hg(NO_3)_2$ at all pH values. As can be seen in Table 1, the rate constant roughly quadruples for every 10 °C

increase in temperature. This behaviour is similar to the work of Van Loon *et al.* (2000).

Whereas Van Loon *et al.* (2000) examined HgO reduction between 6.5 – 35 °C, this work has expanded the temperature range to between 1 – 45 °C (Table 1, Figure S7). Below this range freezing could be possible and above this range the reaction was too rapid for the system to analyze. The enthalpies of activation were determined to be 94 ± 3 kJ mol^{-1} at pH 1 and 92 ± 4 kJ mol^{-1} at pH 3, versus 108 ± 1 kJ mol^{-1} and 105 ± 2 kJ mol^{-1} in the Van Loon *et al.* (2000) results (Table 2). There was a larger discrepancy between the entropies of activation, as in this study the entropies were 33 ± 9 J mol^{-1} K^{-1} at pH 1 and 30 ± 10 J mol^{-1} K^{-1} at pH 3, compared to 81 ± 5 J mol^{-1} K^{-1} and 68 ± 6 J mol^{-1} K^{-1}. The disagreement demonstrates the variability in the intercept of Eyring plots. The error in the rate constant is generally the largest at the temperature extremes, due to relatively short measurement times at lower temperatures and limitation in instrument speed at higher temperatures.

Table 1. Rate constant of Hg^{2+} reduction by sulfite at various temperatures (I < 0.096 M)

HgO				$Hg(NO_3)_2$			
pH	**T (°C)**	**10^3 k (s^{-1})**	**Number of experiments**	**pH**	**T (°C)**	**10^3 k (s^{-1})**	**Number of experiments**
1	1	0.5 ± 0.2	3	**1**	6.5	1 ± 4	2
	6.5	0.9 ± 0.2	7		15.5	3.6 ± 0.5	5
	15.5	3.6 ± 0.3	6		25	13.7 ± 0.5	11
	25	13 ± 8	2		35	53 ± 5	4
	35	49 ± 5	5	**3**	6.5	0.8 ± 0.1	3
	40	92 ± 9	6		15.5	3.1 ± 0.2	6
	45	150 ± 40	3		25	11.8 ± 0.4	4
3	1	0.4 ± 0.8	3		35	42 ± 4	3
	6.5	1.0 ± 0.4	5	**5**	6.5	0.66 ± 0.04	3
	15.5	3.09 ± 0.09	15		15.5	2.6 ± 0.5	4
	25	10 ± 4	3		25	10 ± 1	6
	35	40 ± 10	3		35	40 ± 40	3
	40	87 ± 7	7	**7**	6.5	0.6 ± 0.2	4
	45	120 ± 30	7		15.5	2.63 ± 0.05	4
					25	10 ± 1	12
					35	40 ± 6	3

When $Hg(NO_3)_2$ was used as the source of Hg^{2+} ions, similar results were obtained for the activation parameters (Table 2, Figure 5). The error ranges of the enthalpy and entropy values at pH 1 and pH 3 overlap with their HgO counterparts. The enthalpy and entropy of activation seemingly increased with increasing pH, yet the errors are large enough to consider

this as insignificant. The fact that there is little difference between the parameters for the HgO and $Hg(NO_3)_2$ reactions suggests that these results are applicable to other species of Hg^{2+}. Since more temperatures and Hg^{2+} species were sampled, this work should yield more accurate and reproducible entropy and enthalpy values.

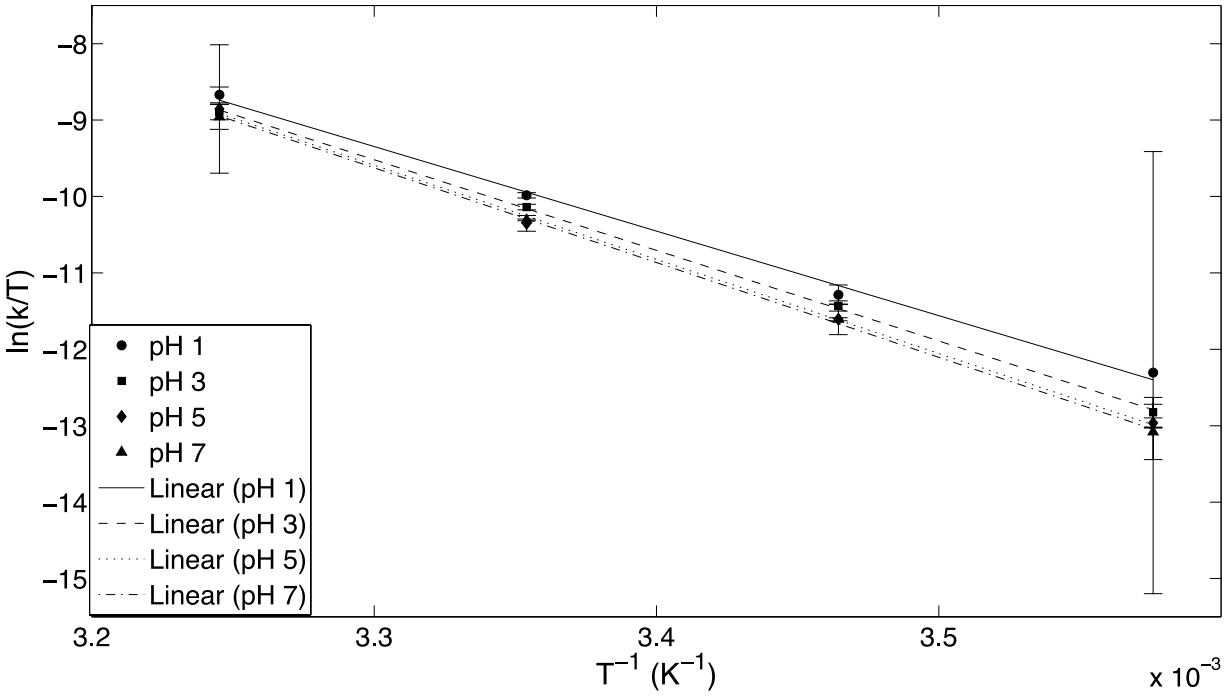

Fig. 5 Eyring plot of experimental temperature-dependent reduction rate constant for $Hg(NO_3)_2$

Table 2. Reaction parameters for the homogeneous reduction of Hg^{2+} by sulfite

	HgO		**$Hg(NO_3)_2$**	
	$\Delta H^{\ddagger}$ (kJ mol^{-1})	$\Delta S^{\ddagger}$ (J mol^{-1} K^{-1})	$\Delta H^{\ddagger}$ (kJ mol^{-1})	$\Delta S^{\ddagger}$ (J mol^{-1} K^{-1})
pH 1	94 ± 3 (108 ± 1)[a]	33 ± 9 (81 ± 5)[a]	92 ± 9	30 ± 30
pH 3	92 ± 4 (105 ± 2)[a]	30 ± 10 (68 ± 6)[a]	99 ± 3	50 ± 10
pH 5	-	-	102 ± 6	60 ± 20
pH 7	-	-	103 ± 3	60 ± 10

[a] Previous work of Van Loon *et al.* (2000)

3.2.3. Ionic Strength Dependence

In the earlier study on the Hg^{2+} reduction reaction by sulfite, ionic strength (0 – 1.1 M $NaClO_4$) was found to have little effect on the rate constant at pH 3 for HgO (Van Loon *et al.*, 2000). However, rates of mercury reactions can be affected by different ions in distinct ways (Hines and Brezonik, 2004; Pehkonen and Lin, 1998). Kinetics experiments were hence conducted with $Hg(NO_3)_2$ using three different ionic species: $NaClO_4$, $NaNO_3$, and KNO_3.

A way of analyzing the effect of ionic strength on the rate constant of a reaction is the primary salt effect. According to the Debye-Hückel theory, an ion in solution is stabilized by surrounding ions of opposite charge (Houston, 2001). The rate constant, k, at ionic strength I, can be described in terms of the rate in the absence of ionic strength, k_0, and the charge of the two species involved in the intermediate, z_A and z_B:

$$\log_{10} k = \log_{10} k_0 + 2Az_A z_B I^{1/2} \qquad (5)$$

where A is a constant equal to 0.50 $(L\ mol^{-1})^{1/2}$. Thus the slope of a $\log(k/k_0)$ vs. $I^{1/2}$ plot should be equal to the multiple of the charges of the two species in the reaction.

The relationship of the reaction at pH 1 to ionic strength contrasts with the behaviour at pH 7 in Figure 6. At pH 1 (Figures 6a-c), the slope of the $\log(k/k_0)$ vs. $I^{1/2}$ plots are indistinguishable from zero for $NaClO_4$ (-0.05 ± 0.1, p = 0.4), and slightly higher for $NaNO_3$ (-0.2 ± 0.3, p = 0.2) and KNO_3 (-0.2 ± 0.2, p = 0.02). However it is apparent from the large errors that the slopes may not be necessarily negative. All of the plots at pH 1 have poor linearity, with $R^2 < 0.09$ for Figures 6a-b, and $R^2 = 0.256$ in Figure 6c. Meanwhile, at pH 7 the slopes are (-0.22 ± 0.04, $p \sim 10^{-13}$) for $NaClO_4$, (-0.31 ± 0.03, $p \sim 10^{-18}$) for $NaNO_3$, and (-0.31 ± 0.02, $p \sim 10^{-19}$) for KNO_3. The R^2 values for these plots are 0.844, 0.949, and 0.963 for $NaClO_4$, $NaNO_3$, and KNO_3. Therefore increasing ionic strength at neutral conditions decelerates the reaction, and the effect is much more reproducible.

There are several possible explanations for the differences in behaviour at pH 1 and pH 7. As stated previously, at pH 1 a charged intermediate $HgSO_3H^+$ is expected to accelerate the reaction. The change in the intermediate's charge can affect the slopes of the plots in Figure 6, as expected from Equation 5 (Houston, 2001). Negative, albeit non-integer, slopes in Figures 6d-f suggest that the reaction at pH 7 involves two oppositely charged species. The poor linearity at pH 1 could be caused by transfer or volume errors, as the reaction rate is sensitive to $[H^+]$ around that pH (Figure S6). At pH 7 the rate constants of replicate trials were more confined. Another

possible source of error is the formation of particles at pH 1. When $NaNO_3$ and KNO_3 were used as the ionic species, particle formation was observed at $I > 0.65$ M in the pH 1 $Hg(NO_3)_2$ solutions. At pH 7 no particle formation was observed, even at $I = 1.2$ M. The influence of heterogeneous conditions could have affected the experiments at pH 1.

For the ionic species tested, the identity of the anion seemed to have the largest effect on kinetics. At pH 1 the slope for $NaClO_4$ in Figure 6 was less in magnitude than that of $NaNO_3$ and KNO_3. KNO_3 had a larger effect on the rate than $NaNO_3$, which could be due to the lower solubility of KNO_3, making those solutions more susceptible to particle formation (Haynes, 2012). At pH 7, the effect of the two nitrate compounds was very similar, suggesting that particle formation was not likely a significant factor at this pH. Further quantification and characterization of the particles formed under acidic conditions is required to determine if particle formation is the influencing factor in the ionic strength effect.

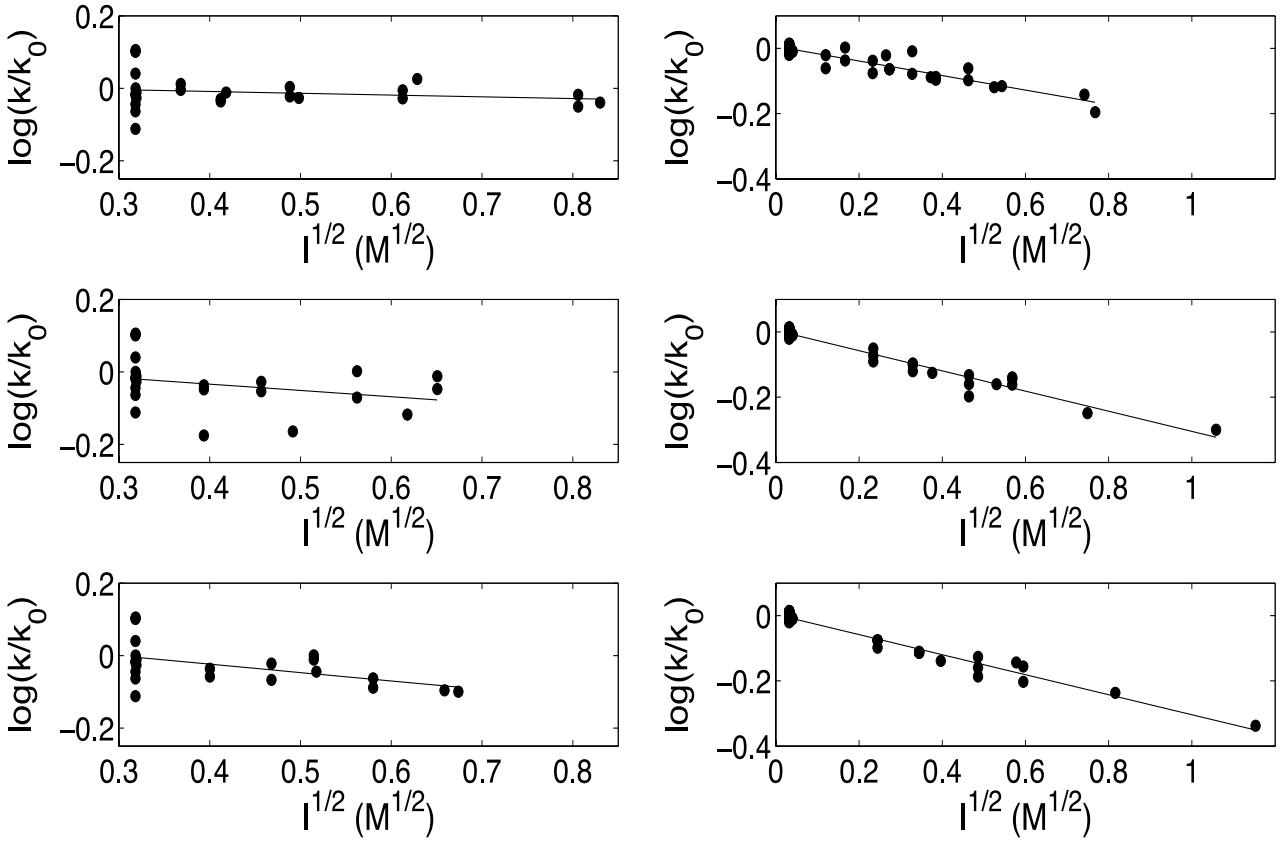

Fig. 6 Dependence of the rate constant on ionic strength at pH 1 in A) $NaClO_4$ B) $NaNO_3$ C) KNO_3 and at pH 3 in D) $NaClO_4$ E) $NaNO_3$ F) KNO_3 at 25 °C for $Hg(NO_3)_2$

At pH 7, the ionic strength behaviour cannot be described solely in terms of the primary salt effect. If this were true, there should be no difference in slope between the two nitrate complexes and $NaClO_4$ (Figure 6). However, the nitrate ion species had a greater effect than $NaClO_4$ in decelerating the rate of Hg^{2+} reduction. More experimental work is required with other ions to determine the cause of the differing behaviour. The effect of chloride ions, which are abundant in aqueous environments, should be further investigated. Chloride ions have been found to promote Hg^0 oxidation in solution (Poulain *et al.*, 2007), and they also form complexes with Hg^{2+} that are difficult to reduce (Gårdfeldt and Jonsson, 2003). By changing the ionic strength with more ionic species, one establishes a better understanding of the reaction kinetics over a range of environmental conditions.

The results of the ionic strength dependency experiments help to explain the reduced rate constant when fly ash is present. As we saw previously, Cumberland and Shawnee fly ashes slowed the reaction rate by 40% and 90%, respectively (Figure 4). Ionic strength effects in the fly ash/water mixture could be partly responsible for the slower Hg^{2+} reduction rates. Previous studies have detected leached Na, Mg, Ca, and heavy metals from fly ash (Tong *et al.*, 2014). Figures 6d-f illustrated that higher ionic strength decelerates the reduction at pH 7. Characterization of fly ash leachate is required to determine the ionic species that are present and possibly affect the reaction rate.

4. Conclusions

With an expanded temperature range, the activation parameters of the HgO sulfite reduction at pH 1 and 3 agree fairly well with the only existing previous values (Table 2). There was no statistical difference between the kinetics of $Hg(NO_3)_2$ and HgO, which generalizes the environmental possibilities of the reaction in modelling mercury transformation in the atmosphere and industrial stacks. The pH results indicated that sulfite reduction of Hg^{2+} can occur from pH 1 to pH 7. Whereas previously an insignificant ionic strength effect was detected at pH 3 for HgO, it was determined that increasing ionic strength (especially with nitrate species) slows down the reaction at neutral pH. The effect of ionic strength on the reduction at pH 1 is more difficult to resolve, as particle formation increases experimental errors and further studies are encouraged. For the first time the effect of fly ash on sulfite reduction was examined. Both

types of fly ash decelerated the reduction reaction of mercury, however the decrease in rate was much more extreme for Shawnee fly ash. The reduction of mercury by Cumberland fly ash was independent of whether Na_2SO_3 was added, which suggests that fly ash itself can be a source of sulfite to aqueous environments. FE-SEM/EDS and ELTRA characterization confirmed that Cumberland fly ash particles were rich in sulfur. The high proportion of nanoparticles in the fly ash samples suggests that there are a large number of available surfaces for heterogeneous chemistry. It is hypothesized that the rate decrease in the heterogeneous case is caused by increased ionic strength or adsorption of Hg^{2+} to fly ash. However, future research on different sizes of fly ash, reactive sites, and co-adsorption and competitive adsorption of pollutants are recommended to evaluate this hypothesis or improve it for further modelling studies. These findings impact the current treatment of mercury reduction reactions in models of atmospheric and aqueous systems.

Acknowledgements

We thank to M. Sutton of Tennessee Valley Authority for providing the Cumberland and Shawnee fly ash samples and to Dr. Sewall of McGill University for his help with the Cary 100 spectrophotometer. We are grateful to Natural Science and Engineering Research Council of Canada, Canadian Foundation for Innovation and Environment Canada for financial support.

References

Amirbahman, A., Kent, D.B., Curtis, G.P. & Marvin-DiPasquale, M.C. (2013). Kinetics of homogeneous and surface-catalyzed mercury (II) reduction by iron (II). *Environ. Sci. Technol.*, 47, 7204-7213.

Ariya, P.A., Dastoor, A.P., Amyot, M., Schroeder, W.H., Barrie, L., Anlauf, K., Raofie, F., Ryzhkov, A., Davignon, D. & Lalonde, J. (2004). The Arctic: a sink for mercury. *Tellus, Ser. B*, 56, 397-403.

Ariya, P.A., Peterson, K., Snider, G. & Amyot, M. 2009, Mercury chemical transformations in the gas, aqueous and heterogeneous phases: state-of-the-art science and uncertainties, *Mercury Fate and Transport in the Global Atmosphere*, Springer, pp. 459-501.

Burda, C., Chen, X., Narayanan, R. & El-Sayed, M.A. (2005). Chemistry and properties of nanocrystals of different shapes. *Chem. Rev.*, 105, 1025-1102.

Clever, H.L., Johnson, S.A. & Derrick, M.E. (1985). The solubility of mercury and some sparingly soluble mercury salts in water and aqueous electrolyte solutions. *J. Phys. Chem. Ref. Data*, 14, 631-680.

Davidson, P.W., Myers, G.J. & Weiss, B. (2004). Mercury exposure and child development outcomes. *Pediatrics*, 113, 1023-1029.

Deeds, D.A., Banic, C.M., Lu, J. & Daggupaty, S. (2013). Mercury speciation in a coal‐fired power plant plume: An aircraft‐based study of emissions from the 3640 MW Nanticoke Generating Station, Ontario, Canada. *J. Geophys. Res.: Atmos.*, 118, 4919-4935.

Ebinghaus, R., Kock, H.H., Temme, C., Einax, J.W., Löwe, A.G., Richter, A., Burrows, J.P. & Schroeder, W.H. (2002). Antarctic springtime depletion of atmospheric mercury. *Environ. Sci. Technol.*, 36, 1238-1244.

Engler, R. (1985). Many Bhopals- technology out of control. *Nation*, 240, 488-&.

Eriksen, M., Mason, S., Wilson, S., Box, C., Zellers, A., Edwards, W., Farley, H. & Amato, S. (2013). Microplastic pollution in the surface waters of the Laurentian Great Lakes. *Mar. Pollut. Bull.*, 77, 177-182.

Evans, M.G. & Polanyi, M. (1935). Some applications of the transition state method to the calculation of reaction velocities, especially in solution. *Trans. Faraday Soc.*, 31, 875-894.

Fitzgerald, W.F., Lamborg, C.H. & Hammerschmidt, C.R. (2007). Marine biogeochemical cycling of mercury. *Chem. Rev.*, 107, 641-662.

Fujita, S., Horii, H. & Taniguchi, S. (1973). Pulse radiolysis of mercuric ion in aqueous solutions. *J. Phys. Chem.*, 77, 2868-2871.

Gallego-Urrea, J.A., Tuoriniemi, J., Pallander, T. & Hassellöv, M. (2010). Measurements of nanoparticle number concentrations and size distributions in contrasting aquatic environments using nanoparticle tracking analysis. *Environ. Chem.*, 7, 67-81.

Gårdfeldt, K. & Jonsson, M. (2003). Is bimolecular reduction of Hg (II) complexes possible in aqueous systems of environmental importance. *J. Phys. Chem. A*, 107, 4478-4482.

Haynes, W.M. (2012). *CRC Handbook of Chemistry and Physics*. CRC press.

Hayon, E., Treinin, A. & Wilf, J. (1972). Electronic spectra, photochemistry, and autoxidation mechanism of the sulfite-bisulfite-pyrosulfite systems. SO2-, SO3-, SO4-, and SO5-radicals. *J. Am. Chem. Soc.*, 94, 47-57.

Higginson, W. (1951). 331. The ultra-violet absorption spectra of mercurous perchlorate solutions. *J. Chem. Soc.*, 1438-1443.

Hines, N.A. & Brezonik, P.L. (2004). Mercury dynamics in a small Northern Minnesota lake: water to air exchange and photoreactions of mercury. *Mar. Chem.*, 90, 137-149.

Houston, P. (2001). *Chemical Kinetics and Reaction Dynamics*. McGraw-Hill Higher Education, New York, NY.

Huang, C. & Blankenship, D. (1984). The removal of mercury (II) from dilute aqueous solution by activated carbon. *Water Res.*, 18, 37-46.

Kutchko, B.G. & Kim, A.G. (2006). Fly ash characterization by SEM–EDS. *Fuel*, 85, 2537-2544.

Lamborg, C.H., Fitzgerald, W.F., O'Donnell, J. & Torgersen, T. (2002). A non-steady-state compartmental model of global-scale mercury biogeochemistry with interhemispheric atmospheric gradients. *Geochim. Cosmochim. Acta*, 66, 1105-1118.

Malisoff, W.M. & Anding Jr, C.E. (1935). Determination of Mercaptans in Hydrocarbon Solvents: An Improvement of the Silver Nitrate Method. *Ind. Eng. Chem., Anal. Ed.*, 7, 86-88.

Morel, F.M., Kraepiel, A.M. & Amyot, M. (1998). The chemical cycle and bioaccumulation of mercury. *Annu. Rev. Ecol. Syst.*, 543-566.

Munthe, J., Xiao, Z. & Lindqvist, O. (1991). The aqueous reduction of divalent mercury by sulfite. *Water, Air, Soil Pollut.*, 56, 621-630.

Namasivayam, C. & Kadirvelu, K. (1999). Uptake of mercury (II) from wastewater by activated carbon from an unwanted agricultural solid by-product: coirpith. *Carbon*, 37, 79-84.

Pehkonen, S.O. & Lin, C.-J. (1998). Aqueous photochemistry of mercury with organic acids. *J. Air Waste Manage. Assoc.*, 48, 144-150.

Pósfai, M., Anderson, J.R., Buseck, P.R. & Sievering, H. (1999). Soot and sulfate aerosol particles in the remote marine troposphere. *J. Geophys. Res.: Atmos.*, 104, 21685-21693.

Poulain, A.J., Garcia, E., Amyot, M., Campbell, P.G., Raofie, F. & Ariya, P.A. (2007). Biological and chemical redox transformations of mercury in fresh and salt waters of the high arctic during spring and summer. *Environ. Sci. Technol.*, 41, 1883-1888.

Selin, N.E. (2014). Global change and mercury cycling: Challenges for implementing a global mercury treaty. *Environ. Toxicol. Chem.*, 33, 1202-1210.

Sen, A.K. & De, A.K. (1987). Adsorption of mercury (II) by coal fly ash. *Water Res.*, 21, 885-888.

Senior, C.L., Sarofim, A.F., Zeng, T., Helble, J.J. & Mamani-Paco, R. (2000). Gas-phase transformations of mercury in coal-fired power plants. *Fuel Process. Technol.*, 63, 197-213.

Tong, Y., Eichhorst, T., Olson, M.R., Rutter, A.P., Shafer, M.M., Wang, X. & Schauer, J.J. (2014). Comparison of heterogeneous photolytic reduction of Hg (II) in the coal fly ashes and synthetic aerosols. *Atmos. Res.*, 138, 324-329.

Van Loon, L., Mader, E. & Scott, S.L. (2000). Reduction of the aqueous mercuric ion by sulfite: UV spectrum of HgSO3 and its intramolecular redox reaction. *J. Phys. Chem. A*, 104, 1621-1626.

Vassilev, S.V. & Vassileva, C.G. (2007). A new approach for the classification of coal fly ashes based on their origin, composition, properties, and behaviour. *Fuel*, 86, 1490-1512.

Wiatrowski, H.A., Das, S., Kukkadapu, R., Ilton, E.S., Barkay, T. & Yee, N. (2009). Reduction of Hg (II) to Hg (0) by magnetite. *Environ. Sci. Technol.*, 43, 5307-5313.

Wilcox, J., Rupp, E., Ying, S.C., Lim, D.-H., Negreira, A.S., Kirchofer, A., Feng, F. & Lee, K. (2012). Mercury adsorption and oxidation in coal combustion and gasification processes. *Int. J. Coal Geol.*, 90, 4-20.

Yardim, M., Budinova, T., Ekinci, E., Petrov, N., Razvigorova, M. & Minkova, V. (2003). Removal of mercury (II) from aqueous solution by activated carbon obtained from furfural. *Chemosphere*, 52, 835-841.

The kinetics of aqueous mercury(II) reduction by sulfite over an array of environmental conditions

Aryeh I. Feinberg, Uday Kurien and Parisa A. Ariya*

Department of Chemistry and Department of Atmospheric and Oceanic Sciences, McGill University

801 Sherbrooke St. W., Montreal, QC, CANADA, H3A 2K6

Tel: (514) 398-6931 Fax: (514) 398-3797

Emails: aryeh.feinberg@mail.mcgill.ca; uday.kurien@mail.mcgill.ca; parisa.ariya@mcgill.ca

** Corresponding author*

Supplementary Information

Error Analysis and Statistical Methods

The average rate constants are given with the standard error of the mean. Derived values such as the acid dependence, entropy and enthalpy are reported with errors propagated from the regression errors. The *p*-values are calculated by the student's t-test. Effects were determined to be statistically insignificant if they could not be distinguished at the 95% confidence level. All errors are reported at 95% confidence level.

For the individual rate constants, a conservative estimate for the error in the fit is 20%. Additional sources of error include the temperature fluctuation, which is about 0.2 °C for each experiment. Since we found that the rate constant quadruples for each 10°C in temperature, there is an additional error of ~10%. Thus the total cumulative error in rate constants would be $(0.2^2 + 0.1^2)^{1/2} = 0.25$, meaning each individual rate constant should be taken with 25% error.

Kinetics investigation using UV absorption spectroscopy

Upon adding sulfite to the mercuric ion solution, a new compound can be detected almost immediately in the UV spectrum. This compound is expected to be $HgSO_3$, forming according to the following reaction (Van Loon et al., 2000):

$$Hg^{2+}_{(aq)} + HSO_3^-{}_{(aq)} \rightarrow HgSO_{3(aq)} + H^+ \qquad (S1)$$

The UV spectrum of $HgSO_3$ is shown in Figure S1. The absorbance peak of $HgSO_3$ is 234 nm, corresponding to the ligand-to-metal charge transfer band of a metal-sulfur coordination complex (Spitzer and Van Eldik, 1982). Koshy and Harris (1983) found a similar peak at 234 nm for the sulfito transition metal complex $Pt(NH_3)_3(SO_3)$. The UV spectrum of the expected product, Hg_2^{2+}, is also displayed in Figure S1.

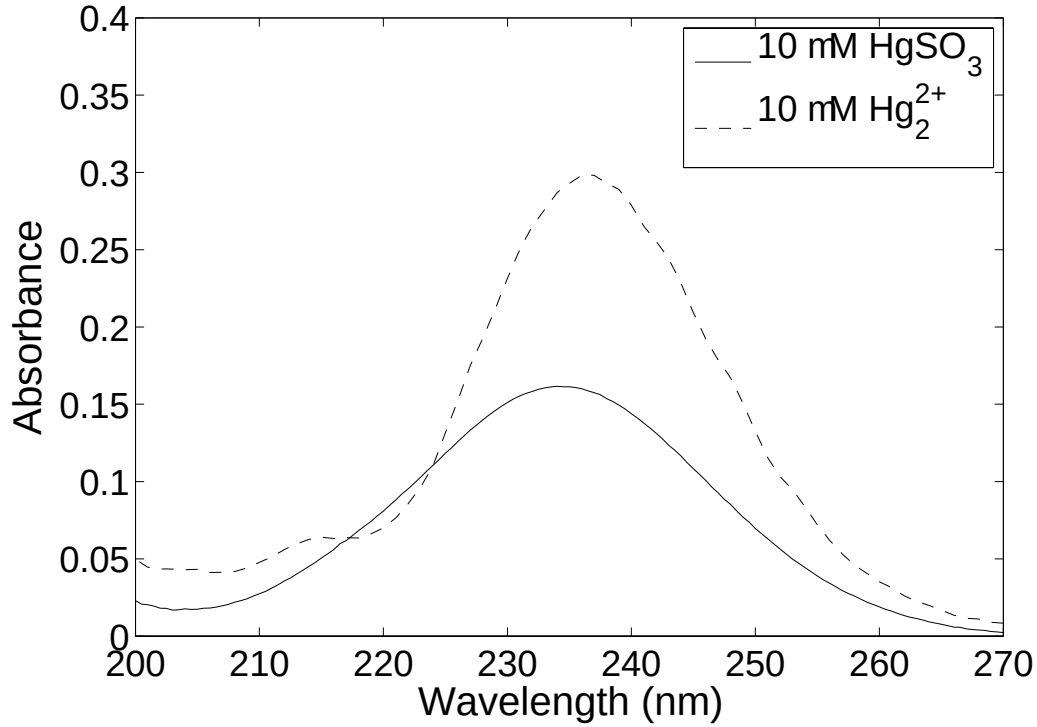

Fig. S1 UV spectra of 10 μM $HgSO_3$ and Hg_2^{2+} at pH 3 ($HClO_4$)

After mixing sulfite with the Hg^{2+} solution, the UV spectrum evolves over time (Figure S2) as $HgSO_3$ is reduced to Hg_2^{2+}. The maximum of the spectrum shifts from 234 nm to 236 nm and peaks appear at 205 nm and 215 nm. These peaks are also present in the Hg_2^{2+} spectrum in Figure S1. There are two clear isosbestic points at 219 and 224 nm. The presence of isosbestic points confirms that the stoichiometry of the reactant must equal that of the product (Moore, 1961). For the absorbance at these points to remain the same throughout the transformation, there must be a one-to-one stoichiometric conversion between $HgSO_3$ and Hg_2^{2+} (Anslyn and Dougherty, 2006).

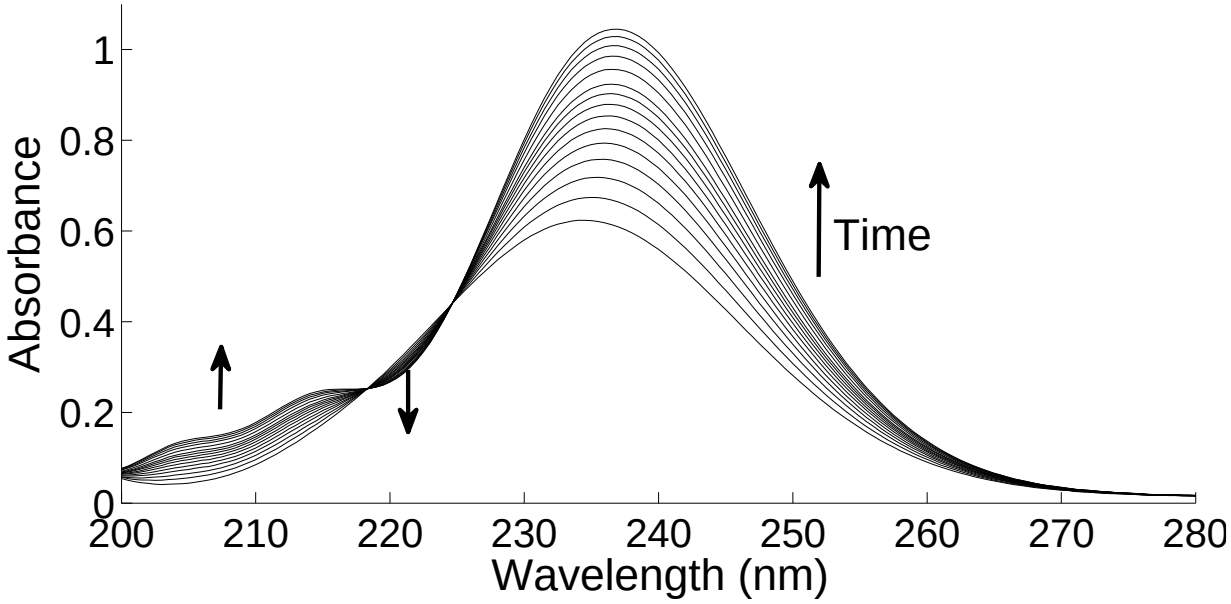

Fig. S2 Evolution of 44 μM $HgSO_3$ in 330 μM Hg^{2+} at pH 3 ($HClO_4$) and 15.5 °C

The extinction coefficients of $HgSO_3$ and its decomposition product were determined by varying the amount of sulfite added to the HgO and $Hg(NO_3)_2$ solutions. The initial absorbance at 234 nm, A_0 in the Equation 1, was taken to be the absorbance of $HgSO_3$ and A_∞ at 236 nm was used as the absorbance of the decomposition product. The linearity of both plots (Figure S3) was high, with $R^2 > 0.997$. This confirms that similar products are forming for both HgO and $Hg(NO_3)_2$. As seen in Figure S3A, ϵ(234 nm) = (1.39 ± 0.04) × 10^4 M^{-1} cm^{-1} for $HgSO_3$. This value, within the experimental cumulative errors, agrees with the extinction coefficient obtained by Van Loon et al. (2000), (1.57 ± 0.05) × 10^4 M^{-1} cm^{-1}. For the product of decomposition, ϵ (236 nm) = (2.39 ± 0.08) × 10^4 M^{-1} cm^{-1} (Figure S3B), which is slightly lower than the previously determined extinction coefficient, (2.74 ± 0.09) × 10^4 M^{-1} cm^{-1} (Van Loon et al., 2000). The literature extinction coefficient of Hg_2^{2+} is (2.4 ± 0.2) × 10^4 M^{-1} cm^{-1}, further supporting that this is the decomposition product (Fujita et al., 1973).

The disparity between the literature extinction coefficients and the values obtained in this work could be due to the trace metal catalyzed autoxidation of sulfite (Hayon et al., 1972; Van Loon et al., 2000). If the sulfite were partly oxidized by air, the added concentration of reactive sulfite would be overestimated. However, precautions were taken to avoid autoxidation, such as preparing the sulfite solution fresh daily and storing the solution in an airtight vial. These

precautions were seemingly effective, as A_0 and A_∞ for the same amount of sulfite added did not change significantly over a day of experiments.

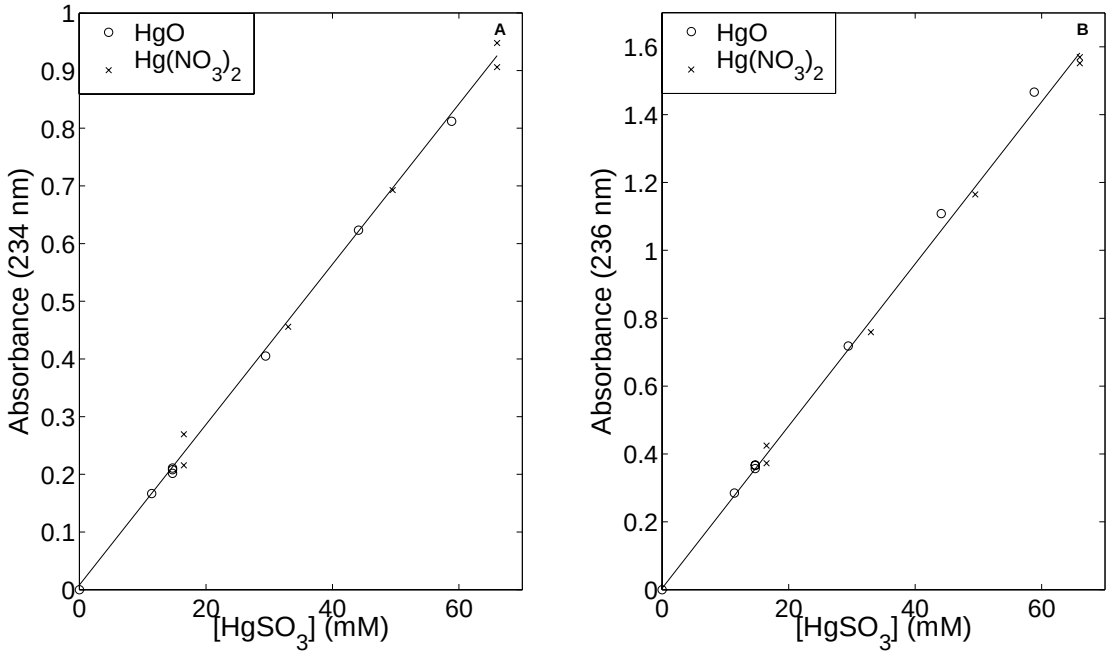

Fig. S3 Extinction coefficients of A) $HgSO_3$ and B) the reaction product at pH 3 ($HClO_4$) and 15.5 °C

By monitoring the absorbance at 236 nm, kinetic profiles of the Hg^{2+} reduction were constructed (Figure S4). The first order rate constant was independent of the sulfite concentration and the concentration of Hg^{2+}. The rate of reaction was also insensitive to the solution being air-saturated or argon-saturated (Figure S4), which suggests that sulfite radicals are not involved (Houston, 2001; Van Loon et al., 2000). Since the rate constant is first order, we have (Van Loon et al., 2000):

$$-\frac{d[\mathrm{HgSO_3}]}{dt} = k_0[\mathrm{HgSO_3}] \qquad \text{(S2)}$$

Using HgO as the initial reagent, the rate constant at 25.0 °C, pH 3, and ionic strength I = 0.0023 M is $k_0 = (0.010 \pm 0.004)\ s^{-1}$, which agrees with the Van Loon et al. (2000) value of $(0.0106 \pm 0.0009)\ s^{-1}$. A similar rate constant is obtained with $Hg(NO_3)_2$, $k_0=(0.0118 \pm 0.0004)\ s^{-1}$.

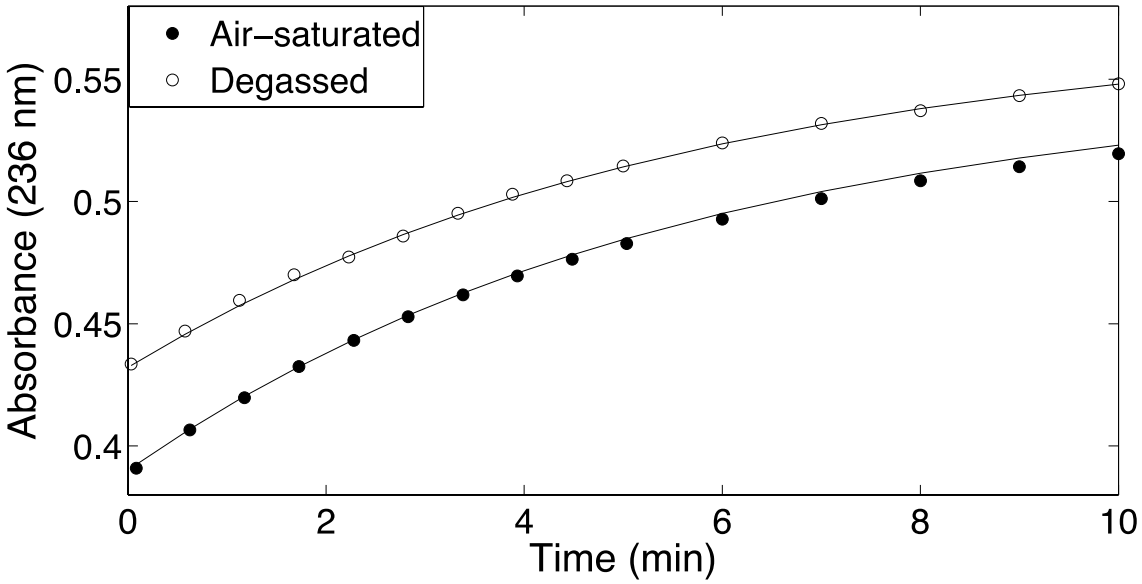

Fig. S4 Kinetic profiles of Hg^{2+} reduction in air-saturated and degassed HgO solutions at 15.5 °C and pH 3 (the data are offset for better viewing)

Physical/Chemical Characterization of Fly Ash

To illustrate that some particles in the sample are iron rich, an additional FE-SEM image is provided below.

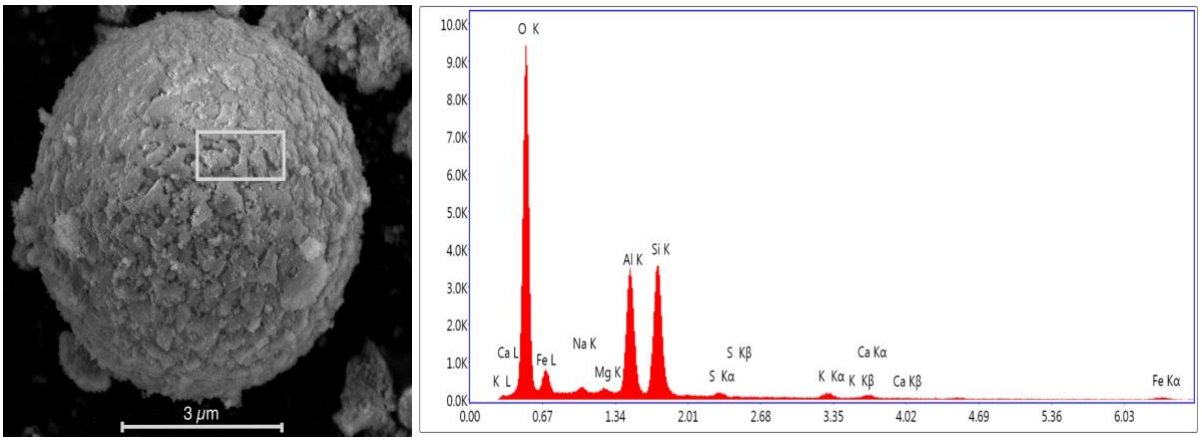

Fig. S5 FE-SEM image/EDS spectrum of Cumberland ash particle containing mainly, by weight %, O, Si, Al and Fe

Homogeneous Reduction of Hg(II) by sulfite

In the presence of acid, one can alter the expression of the rate constant to yield (Van Loon *et al.*, 2000):

$$k = k_0 + k_1 [H^+] \qquad \text{(S3)}$$

From the data in Figure S6, $k_0 = (0.010 \pm 0.002)$ s^{-1} and $k_1 = (0.010 \pm 0.003)$ M^{-1} s^{-1} at 25.0 °C. Therefore the acid-catalyzed path will contribute significantly > 5% to the overall rate constant at low pH values (< 1.3).

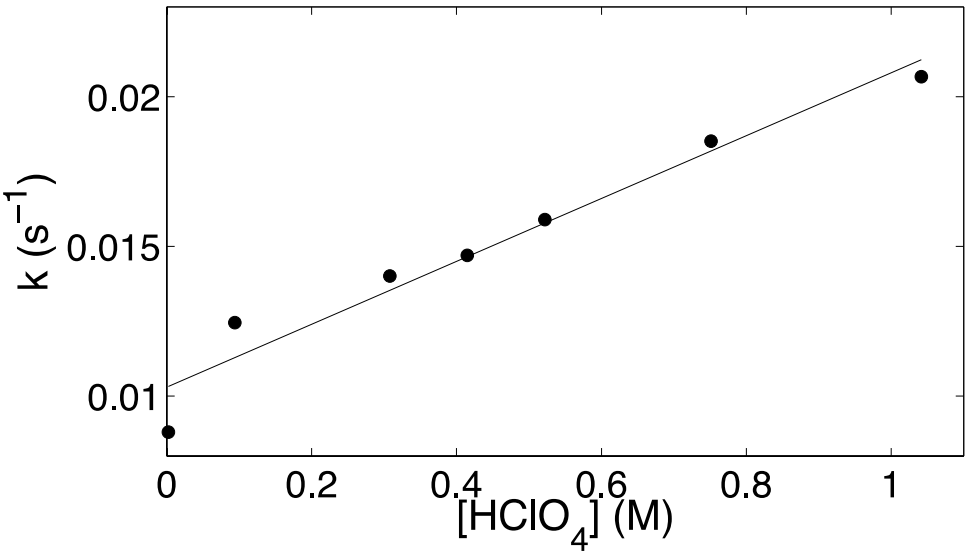

Fig. S6 Rate constant versus pH at I = 1.0-1.1 M ($HClO_4/NaClO_4$) with HgO as the Hg^{2+} species

Temperature Dependence

In this experiment, the temperature range was expanded to 1 – 45 °C. The data in Figure S7 for HgO can be compared to Figure 7 in the paper by Van Loon et al. (2000). Their data corresponds to a temperature range of 6.5 – 35 °C.

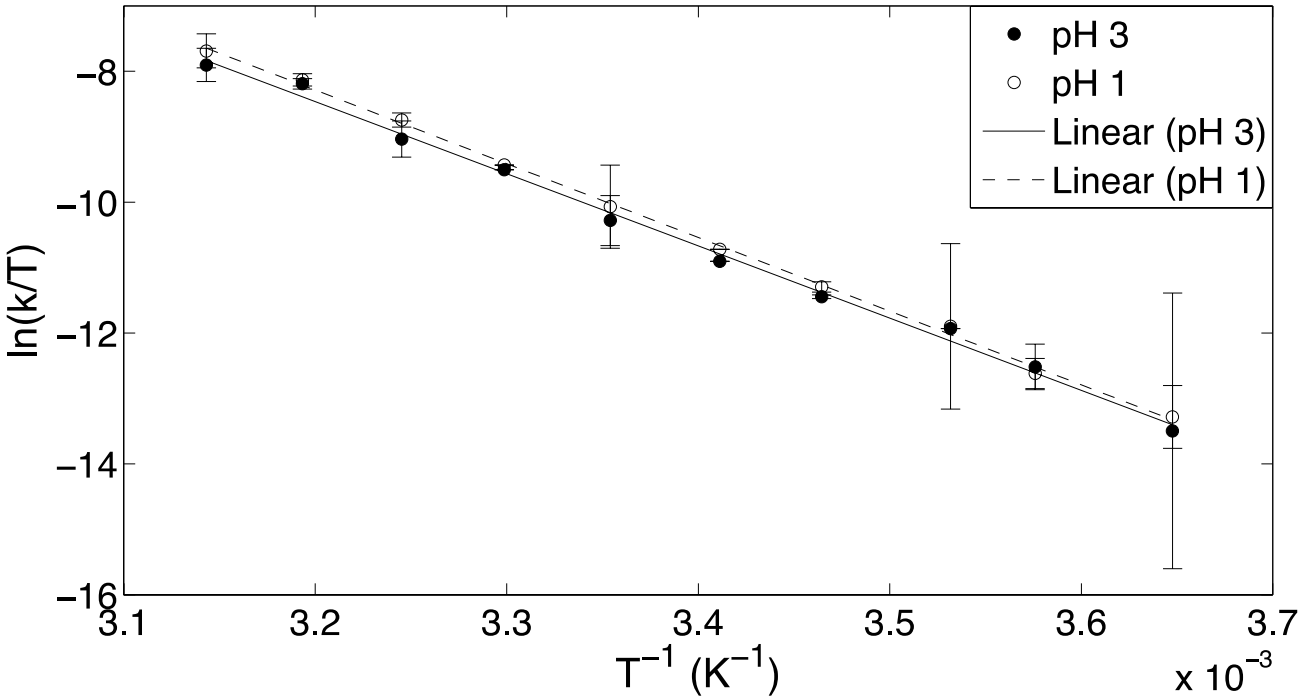

Fig. S7 Eyring plot of experimental temperature-dependent reduction rate constant for HgO

ELTRA CS-800 Analysis of Sulfur Content

The analysis of fly ash sulfur content by ELTRA CS-800 is shown in figure S8. The errors were less than 5% (1σ) based on replicates of the standards.

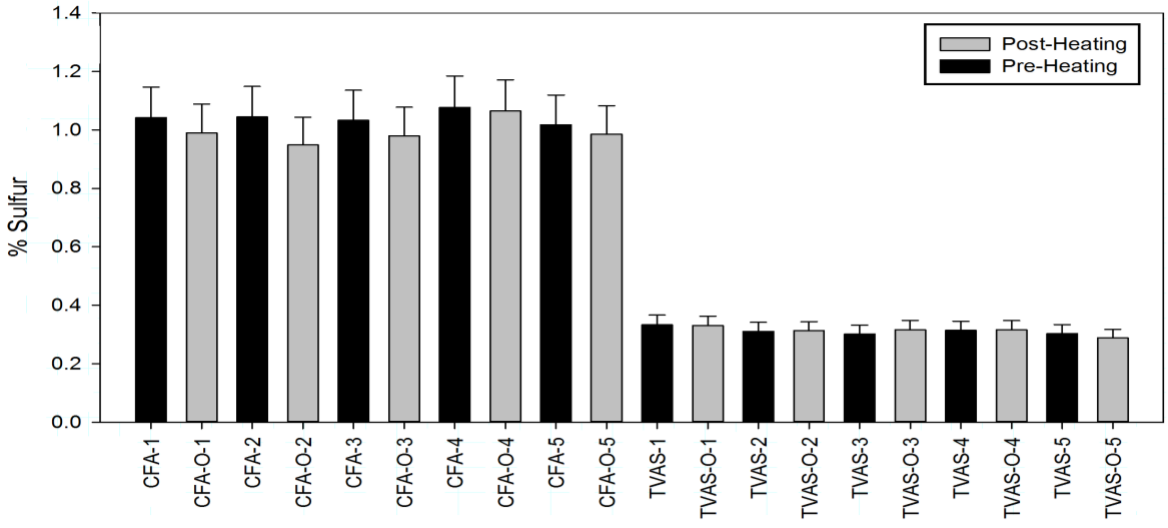

Fig. S8 ELTRA analysis of fly ash sulfur content. (CFA – Cumberland Fly Ash, TVAS-Shawnee Fly Ash, 'O' refers to oven heated sample)

References

Anslyn, E.V. & Dougherty, D.A. (2006). *Modern Physical Organic Chemistry*. University Science Books.

Fujita, S., Horii, H. & Taniguchi, S. (1973). Pulse radiolysis of mercuric ion in aqueous solutions. *J. Phys. Chem.*, 77, 2868-2871.

Hayon, E., Treinin, A. & Wilf, J. (1972). Electronic spectra, photochemistry, and autoxidation mechanism of the sulfite-bisulfite-pyrosulfite systems. SO2-, SO3-, SO4-, and SO5-radicals. *J. Am. Chem. Soc.*, 94, 47-57.

Houston, P. (2001). *Chemical Kinetics and Reaction Dynamics*. McGraw-Hill Higher Education, New York, NY.

Koshy, K. & Harris, G. (1983). Kinetics and mechanism of the reactions of sulfito complexes in aqueous solution. 5. Formation, isomerization and sulfite addition reactions of the oxygen-bonded (sulfito) pentaammineplatinum (IV) ion and the subsequent intramolecular redox reactions of the sulfur-bonded intermediate, the cis-bis (sulfito) tetraammineplatinum (IV) ion. *Inorg. Chem.*, 22, 2947-2953.

Moore, J.W. (1961). *Kinetics and Mechanism*. John Wiley & Sons.

Spitzer, U. & Van Eldik, R. (1982). Kinetics and mechanisms of the formation, substitution, and aquation reactions of sulfur-bonded (sulfito) amminecobalt (III) complexes in aqueous solution. *Inorg. Chem.*, 21, 4008-4014.

Van Loon, L., Mader, E. & Scott, S.L. (2000). Reduction of the aqueous mercuric ion by sulfite: UV spectrum of HgSO3 and its intramolecular redox reaction. *J. Phys. Chem. A*, 104, 1621-1626.